AD-A063 708 AEROSPACE CORP EL SEGUNDO CALIF F/G 20/4

EVALUATION OF TOTAL HEAT TRANSFER IN HYPERSONIC FLOW ENVIRONMEN--ETC(U)

OCT 78 R L BAKER, R F KRAMER F04701-77-C-0078

UNCLASSIFIED TR-0078(3550-15)-3 SAMSO-TR-78-20 NL

1 OF 1

AD
A063708

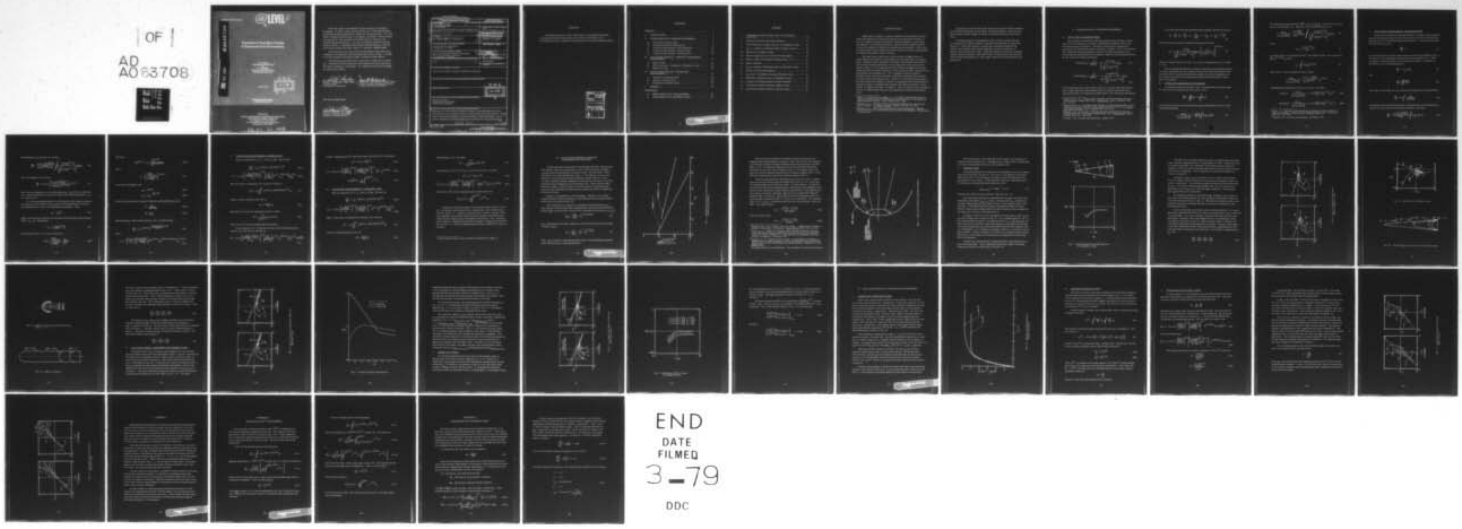

END
DATE
FILMED
3-79
DDC

REPORT SAMSO-TR-78-20

(12) LEVEL II

AD A063708

DDC FILE COPY

Evaluation of Total Heat Transfer in Hypersonic Flow Environments

R. L. BAKER
Vehicle Engineering Division
and
R. F. KRAMER
Information Processing Division
The Aerospace Corporation

DDC
RECEIVED
JAN 24 1979
B

October 1978

APPROVED FOR PUBLIC RELEASE;
DISTRIBUTION UNLIMITED

Prepared for

SPACE AND MISSILE SYSTEMS ORGANIZATION
AIR FORCE SYSTEMS COMMAND
Los Angeles Air Force Station
P.O. Box 92960, Worldway Postal Center
Los Angeles, Calif. 90009

79 01 22 069

This final report was submitted by The Aerospace Corporation, El Segundo, CA 90245, under Contract F04701-77-C-0078 with the Space and Missile Systems Organization, Deputy for Reentry Systems, P.O. Box 92960, Worldway Postal Center, Los Angeles, CA 90009. It was reviewed and approved for The Aerospace Corporation by E.G. Hertler of the Vehicle Engineering Division, A.R. Sims of the Information Processing Division, and R. L. Strickler of the Reentry Systems Division. The Air Force project officer was Capt. Robert J. Chambers, SAMSO/RSSE.

This report has been reviewed by the Information Office (OI) and is releasable to the National Technical Information Service (NTIS). At NTIS, it will be available to the general public, including foreign nations.

This technical report has been reviewed and is approved for publication. Publication of this report does not constitute Air Force approval of the report's findings or conclusions. It is published only for the exchange and stimulation of ideas.

Robert J. Chambers, Capt. USAF
Project Officer
Aerothermal Technology

James M. McCormack, Lt. Col. USAF
Chief, Reentry Technology Division
Deputy for Reentry Systems

FOR THE COMMANDER

William Goldberg, Col. USAF
Director, Systems Technology
Deputy for Reentry Systems

UNCLASSIFIED

SECURITY CLASSIFICATION OF THIS PAGE (When Data Entered)

(19) **REPORT DOCUMENTATION PAGE**

READ INSTRUCTIONS BEFORE COMPLETING FORM

1. REPORT NUMBER (18) SAMSO-TR-78-20

2. GOVT ACCESSION NO.

3. RECIPIENT'S CATALOG NUMBER

4. TITLE (and Subtitle) (6) Evaluation of Total Heat Transfer in Hypersonic Flow Environments.

5. TYPE OF REPORT & PERIOD COVERED
Final
8-1-76 through 6-30-78

6. PERFORMING ORG. REPORT NUMBER (14) TR-0078(3550-15)-3

7. AUTHOR(s) (10) R. L. Baker ~~and~~ R. F. Kramer

8. CONTRACT OR GRANT NUMBER(s) (15) F04701-77-C-0078

9. PERFORMING ORGANIZATION NAME AND ADDRESS
The Aerospace Corporation
El Segundo, CA 90245

10. PROGRAM ELEMENT, PROJECT, TASK AREA & WORK UNIT NUMBERS

11. CONTROLLING OFFICE NAME AND ADDRESS
Space and Missile Systems Organization
Air Force Systems Command
Los Angeles, CA 90009

12. REPORT DATE (11) Oct[redacted]978

13. NUMBER OF PAGES
42 (12) 46p.

14. MONITORING AGENCY NAME & ADDRESS (if different from Controlling Office)
(9) Final rept. 1 Aug 76 - 30 Jun 78,

15. SECURITY CLASS. (of this report)
Unclassified

15a. DECLASSIFICATION/DOWNGRADING SCHEDULE

16. DISTRIBUTION STATEMENT (of this Report)

Approved for public release; distribution unlimited.

17. DISTRIBUTION STATEMENT (of the abstract entered in Block 20, if different from Report)

18. SUPPLEMENTARY NOTES

DDC
RECEIVED
JAN 24 1979
B

19. KEY WORDS (Continue on reverse side if necessary and identify by block number)

Reentry vehicles
Hypersonic heat transfer
Nosetip heat transfer

20. ABSTRACT (Continue on reverse side if necessary and identify by block number)

Equations for the total heat transfer to bodies in constant hypersonic flow environments and a ballistic trajectory environment have been derived. Using these equations and graphical results presented, total heat transfer can be easily evaluated for selected sphere-cone and flat-face cone geometries.

009 500 JOB

DD FORM 1473 (FACSIMILE)

UNCLASSIFIED

SECURITY CLASSIFICATION OF THIS PAGE (When Data Entered)

79 01 22 069

PREFACE

The helpful assistance of Mr. Matt Brunner in providing information concerning his earlier work and the work of Dr. Walt Reddall, III in providing the Godunov computer code calculations are acknowledged gratefully.

ACCESSION for
NTIS White Section
DDC Buff Section
UNANNOUNCED
JUSTIFICATION
BY
DISTRIBUTION/AVAILABILITY CODES
Dist. AVAIL. and/or SPECIAL
A

CONTENTS

PREFACE 1

I. INTRODUCTION 5

II. INTEGRATED HEAT TRANSFER EXPRESSIONS 7

A. Local Heat Transfer Rates 7

B. Constant Freestream Environment 8

C. Trajectory Environment--Basic Equations 10

D. Trajectory Environment--Laminar Flow 13

E. Trajectory Environment--Turbulent Flow 14

III. CALCULATED RESULTS--CONSTANT FREESTREAM ENVIRONMENT 17

A. Sphere-Cones 21

B. Flat-Face Cones--Comparison with Sphere-Cones 27

C. Effect of γ and ω 30

IV. CALCULATED RESULTS--TRAJECTORY ENVIRONMENT 35

A. Laminar or Turbulent Flows 35

B. Laminar-Turbulent Flow 37

C. Evaluating Local Heat Loads 38

V. SUMMARY 43

APPENDICES:

A. DERIVATION OF Q^{LT} RELATIONSHIP 45

B. COMPARISON WITH BRUNNER'S WORK 47

FIGURES

1. Nondimensional Heat Transfer Rate as a Function of I_Q and Re_o 18

2. Numerical Flowfield Calculation Methods 20

3. Body Geometries and I_Q^L Values for 10-deg Sphere-Cones . . 22

4. I_Q as a Function of Thickness Ratio for Sphere-Cones 24

5a. I_Q^L versus τ for Sphere-Cones 25

5b. Minimum I_Q^L Cones for Various Cone Half-angles 25

5c. Sphere-Cones with Constant Thickness Ratio, $\tau = 1.3$ 26

5d. Sphere-Cylinder 26

6. I_Q as a Function of Thickness Ratio for Flat-face Cones . . . 28

7. Surface Pressure Distributions 29

8. I_Q versus τ for Sphere-Cones and Flat-face Cones 31

9. Sensitivity of I_Q^L to γ and ω, 10-deg Sphere-Cone 32

10. Laminar and Turbulent Heat Transfer Functions 36

11. Local Heat Transfer Functions, Sphere-Cones 40

12. Local Heat Transfer Function, Flat-face Cones 41

I. INTRODUCTION

Apparently no method is readily available in the published literature which will enable quick and easy evaluation of the total heat transfer to a body in a hypersonic flow environment. Such information is very useful, for example, in evaluating heat sink or internal coolant requirements for various body shapes in a ground test hypersonic environment, or the transpiration-cooled nosetip coolant and reentry vehicle heat shield requirements for ballistic hypersonic reentry vehicles.

The initial work in this area is that of Allen and Eggers (Ref. 1). These authors give the form of an equation for total heat load to a reentry body. However, direct calculation of results is not possible since the convective heat transfer relationship is left unspecified in the final equation. Brunner (Refs. 2, 3) has extended the work of Allen and Eggers by incorporating flat-plate-reference-enthalpy convective heat transfer expressions for both laminar and turbulent flow. For a complete reentry trajectory, Brunner's work allows the evaluation of the total local heat load in Btu/ft^2 at a given station on a sphere-cone. However, to obtain the total heating to the entire body from Brunner's results, an integration must be performed of the given laminar or turbulent heat transfer distribution functions over the sphere, or sphere-cone body, of interest. Also, for sphere-cones, Brunner's results are approximate because of the approximate pressure distribution used.

---

[1] Allen, H. Julian and A.J. Eggers, Jr., "A Study of the Motion and Aerodynamic Heating of Ballistic Missiles Entering the Earth's Atmosphere at High Supersonic Speeds," NACA Report 1381, 1958.

[2] Brunner, M.J., "Analysis of the Aerodynamic Heating for a Re-entrant Space Vehicle," J. of Heat Transfer, August 1959, pp. 223-229.

[3] Brunner, M.J., "Heat Protection System Concept Evaluation," Report PIR U-9190-73-114, General Electric Company, Philadelphia, Pennsylvania, 9 January 1973.

The primary purpose of this work has been to provide analytic equations and calculated numerical results which, when taken together, allow the total heat transfer for body shapes of interest to be quickly and accurately calculated.

Total heat transfer relationships for both constant, ground test type, environments and realistic ballistic trajectory environments are derived in Section II. In the later sections, numerically calculated results for the laminar and turbulent heat transfer integrals are given for families of sphere-cones and flat-face cones. When the numerical results are combined with the analytic equations, total heat transfer in both types of environments may be readily calculated for a wide range of sphere-cone and flat-face cone geometries.

II. INTEGRATED HEAT TRANSFER EXPRESSIONS

A. LOCAL HEAT TRANSFER RATES

An expression is needed for the total integrated heat transfer in hypersonic flow environments as a function of appropriate flowfield, body scale, and body geometry parameters. But first, an appropriate expression is required for the local heat transfer coefficient. In Refs. 4 and 5, the boundary layer integral momentum equation is solved, and Reynolds analogy and a compressibility transformation are applied to obtain the following expressions for the local heat transfer coefficient:

$$(\text{Laminar})C_H = \frac{\dot{q}^L}{\rho_e u_e H_o} = \frac{0.470\, r\mu_e}{\left[2\int_0^s \rho_e u_e \mu_e r^2 ds\right]^{1/2}} \tag{1a}$$

$$(\text{Turbulent})C_H = \frac{\dot{q}^T}{\rho_e u_e H_o} = \frac{0.0288 r^{1/4}\mu_e}{\mu_o^{3/5}\left[\int_0^s \rho_e u_e \mu_e r^{5/4} ds\right]^{1/5}} \tag{1b}$$

These expressions have been found to agree very closely with experimental data at high supersonic Mach numbers (Ref. 6); limited comparison with experimental data for a hypersonic Mach number* also shows good agreement.

---

[4] Vaglio-Laurin, R., "Laminar Heat Transfer on Three-Dimensional Blunt Nosed Bodies in Hypersonic Flow," ARS Journal, 29(2), February 1959, pp. 123-129.

[5] Vaglio-Laurin, R., "Turbulent Heat Transfer on Blunt Nosed Bodies in Two-Dimensional and General Three-Dimensional Hypersonic Flow," J. of the Aero/Space Sciences, 27(1), January 1960, pp. 27-36.

[6] Widhopf, G. F. and R. Hall, "Transitional and Turbulent Heat Transfer Measurements on a Yawed Blunt Conical Nose Tip," AIAA Journal, 10(10), October 1972, pp. 1318-1325.

* Crowell, P.G., private communication, January 1973.

If we define the following nondimensional quantities denoted by the bars

$$\bar{\rho}_e = \frac{\rho_e}{\rho_o}, \ \bar{\mu}_e = \frac{\mu_e}{\mu_o}, \ \bar{u}_e = \frac{u_e}{\sqrt{2H_o}}, \ \bar{r} = \frac{r}{r_B}, \ \bar{s} = \frac{s}{r_B}, \ \tau = \frac{2r_B}{L} \tag{2}$$

then the local heat transfer coefficient expressions become

$$C_H = \frac{C_1 \bar{r}^n \bar{\mu}_e}{\left[\int_0^{\bar{s}} \bar{\rho}_e \bar{u}_e \bar{\mu}_e \bar{r}^{\,n+1} d\bar{s}\right]^{n/(n+1)}} \left\{ \frac{\mu_o}{\rho_o (2H_o)^{1/2} r_B} \right\}^{n/(n+1)} \tag{3}$$

where for laminar flow $C_1 = 0.332$, $n = 1$ and for turbulent flow $C_1 = 0.0288$, $n = 1/4$.

We now distinguish between a constant freestream environment problem for which integration over the surface area gives the total heat transfer rate in Btu/sec and a trajectory environment problem for which integration over the surface area and for all altitudes gives the total heat transfer in Btu's. This is done below.

B. CONSTANT FREESTREAM ENVIRONMENT

To obtain the total heat transfer rate, we integrate the local heat transfer rate $\dot{q}$ over the surface area of the body. Thus

$$\frac{dQ}{dt} = \iint_S \dot{q} dS = 2\pi \int_0^s \dot{q} r ds \tag{4}$$

The total heat transfer rate then becomes upon substituting from Eq. (1) and nondimensionalizing

$$\frac{dQ/dt}{\rho_\infty V_\infty H_o \left(\pi r_B^2\right)} = 2\left(\frac{\gamma+1}{\gamma-1}\right) \int_0^{\bar{s}} \bar{\rho}_e \bar{u}_e C_H \bar{r} d\bar{s} \tag{5}$$

The hypersonic approximations $\sqrt{2H_o} \approx V_\infty$ and $\rho_o/\rho_\infty = (\gamma+1)/(\gamma-1)$ have been made in obtaining Eq. (5). When Eq. (3) is substituted into Eq. (5)

$$\frac{dQ/dt}{\rho_\infty V_\infty H_o\left(\pi r_B^2\right)} = \frac{2C_1\left(\frac{\gamma+1}{\gamma-1}\right)}{[Re_o]^{n/(n+1)}} \int_0^{\bar{s}} \frac{\bar{\rho}_e \bar{u}_e \bar{\mu}_e \bar{r}^{n+1} d\bar{s}}{\left[\int_0^{\bar{s}} \bar{\rho}_e \bar{u}_e \bar{\mu}_e \bar{r}^{n+1} ds\right]^{n/(n+1)}} \tag{6}$$

where

$$Re_o = \frac{\rho_o (2H_o)^{1/2} r_B}{\mu_o} \tag{7}$$

As noted in Ref. 7 (and footnote below*), the integral in Eq. (6) is of the form $\int [I_Q]^{-n/(n+1)} dI_Q$ where

$$I_Q = \int_0^{\bar{s}} \bar{\rho}_e \bar{u}_e \bar{\mu}_e \bar{r}^{n+1} d\bar{s} \tag{8}$$

Thus, Eq. (6) may be integrated once to obtain

$$\frac{dQ/dt}{\rho_\infty V_\infty H_o\left(\pi r_B^2\right)} = \frac{2(n+1)\, C_1\left(\frac{\gamma+1}{\gamma-1}\right)}{[Re_o]^{n/(n+1)}}\, I_Q^{\,1/(n+1)} \tag{9}$$

Substituting the appropriate values for C_1 and n, we obtain

$$\text{(Laminar)} \quad \frac{dQ^L/dt}{\rho_\infty V_\infty H_o\left(\pi r_B^2\right)} = 1.328\left(\frac{\gamma+1}{\gamma-1}\right)\left(I_Q^L\right)^{1/2} Re_o^{-1/2} \tag{10a}$$

$$\text{(Turbulent)} \quad \frac{dQ^T/dt}{\rho_\infty V_\infty H_o\left(\pi r_B^2\right)} = 0.0720\left(\frac{\gamma+1}{\gamma-1}\right)\left(I_Q^T\right)^{4/5} Re_o^{-1/5} \tag{10b}$$

---

[7] Aihara, Y., "Optimum Body Geometries of Minimum Heat Transfer at Hypersonic Speeds," AIAA Journal, Technical Notes, 6(11), November 1968, pp. 2187-2188.

*Crowell, P.G., private communication, November 1976.

C. TRAJECTORY ENVIRONMENT--BASIC EQUATIONS

In this case to obtain the total heat transfer, we must not only integrate the local heat transfer rate over the surface area of the body, but must also integrate in time (or altitude) through the trajectory. If we let $\mathscr{H}$ = total heat transfer/unit area, then

$$\frac{d\mathscr{H}}{dt} = \dot{q} \tag{11}$$

The development here closely follows that given by Allen and Eggers (Ref. 1) except that a key simplifying assumption has been eliminated; i.e., Allen and Eggers assumed that Re_o is not a function of altitude. If altitude is denoted by y, to a good approximation

$$\frac{dy}{dt} = -V_\infty \sin\theta_E \tag{12}$$

also

$$\frac{dQ}{dy} = \iint_S \frac{d\mathscr{H}}{dy}\, dS \tag{13}$$

After Eqs. (11) through (13) are combined and integrated circumferentially

$$\frac{dQ}{dy} = 2\pi \int_0^s \frac{-\dot{q} r ds}{V_\infty \sin\theta_E} \tag{14}$$

Proceeding with nondimensionalization, approximations and simplifications exactly as in the constant environment case above, we obtain

$$\frac{dQ}{dy} = \frac{-\rho_\infty V_\infty^2 \pi r_B^2 \left(\frac{\gamma+1}{\gamma-1}\right)}{\sin\theta_E} \int_0^{\bar{s}} \bar{\rho}_e \bar{u}_e C_H \bar{r}\, d\bar{s} \tag{15}$$

Substituting for C_H from Eq. (3), we find

$$\frac{dQ}{dy} = \frac{-C_1 \rho_\infty V_\infty^2 \pi r_B^2 \left(\frac{\gamma+1}{\gamma-1}\right)}{[Re_o]^{n/(n+1)} \sin\theta_E} \int_0^{\bar{s}} \frac{\bar{\rho}_e \bar{u}_e \bar{\mu}_e \bar{r}^{n+1} d\bar{s}}{\left[\int_0^{\bar{s}} \bar{\rho}_e \bar{u}_e \bar{\mu}_e \bar{r}^{n+1} d\bar{s}\right]^{n/(n+1)}} \tag{16}$$

When we integrate in $\bar{s}$ as before

$$\frac{dQ}{dy} = -(n+1)C_1 \left[\frac{\rho_\infty V_\infty^2 \pi r_B^2 \left(\frac{\gamma+1}{\gamma-1}\right)}{\sin\theta_E [Re_o]^{n/(n+1)}}\right] I_Q^{1/(n+1)} \tag{17}$$

Before we can integrate in y, we must express ρ_∞, V_∞ and Re_o as functions of y. Notice that because of the way in which it is nondimensionalized, I_Q is not a function of y.

To a very good approximation, the viscosity over the range of pressure and temperature of interest may be assumed to be independent of pressure and represented by a power law temperature dependence. Thus

$$\mu_o = C_\mu T_o^\omega \tag{18}$$

When we use ideal gas expressions and employ the hypersonic approximation $\sqrt{2H_o} = V_\infty$, Eq. (18) becomes

$$\mu_o = C_\mu \left(\frac{\gamma-1}{2\gamma R}\right)^\omega V_\infty^{2\omega} \tag{19}$$

Substituting into Eq. (7), we may write Re_o as

$$Re_o = \frac{\left(\frac{\gamma+1}{\gamma-1}\right) r_B}{C_\mu \left(\frac{\gamma-1}{2\gamma R}\right)^\omega} \frac{\rho_\infty}{V_\infty^{2\omega-1}} \tag{20a}$$

Therefore

$$Re_o^{n/(n+1)} = C_2 \frac{\rho_\infty^{n/(n+1)}}{V_\infty^{(2\omega-1)n/(n+1)}} \tag{20b}$$

where

$$C_2 = \left[\frac{\left(\frac{\gamma+1}{\gamma-1}\right) r_B}{C_\mu \left(\frac{\gamma-1}{2\gamma R}\right)^\omega} \right]^{n/(n+1)} \tag{21}$$

From Allen and Eggers work

$$\rho_\infty = \rho^o e^{-\lambda y} \tag{22a}$$

$$V_\infty = V_E e^{-\frac{B}{2} e^{-\lambda y}} \tag{22b}$$

where the ballistic factor B and the ballistic coefficient β are given by

$$B = \frac{\rho^o}{\lambda \beta \sin\theta_E} \tag{23a}$$

$$\beta = \frac{m}{C_D A} \tag{23b}$$

Substituting Eqs. (20b) and (22) into Eq. (17), we obtain finally

$$\frac{dQ}{dy} = C_3 e^{-\lambda y/(n+1)} e^{-\frac{[(2\omega+1)n+2]B}{2(n+1)} e^{-\lambda y}} \tag{24}$$

where

$$C_3 = -\left\{ \frac{(n+1)C_1}{C_2} \right\} \left[\frac{\pi r_B^2 \left(\frac{\gamma+1}{\gamma-1}\right)}{\sin\theta_E} \right] \rho^{o\,1/(n+1)} V_E^{[(2\omega+1)n+2]/(n+1)} I_Q^{1/(n+1)} \tag{25}$$

D. TRAJECTORY ENVIRONMENT--LAMINAR FLOW

When we substitute for n, C_1, and C_2 in Eqs. (24) and (25)

$$\frac{dQ^L}{dy} = C_3^L e^{-(\lambda/2)y} e^{-(2\omega+3)B/4} e^{-\lambda y} \tag{26a}$$

$$C_3^L = -0.939 \left[\frac{C_\mu \left(\frac{\gamma-1}{2\gamma R}\right)^\omega \left(\frac{\gamma+1}{\gamma-1}\right)}{r_B} \right]^{1/2} \left[\frac{\pi r_B^2}{\sin\theta_E} \right] \rho_o^{1/2} V_E^{(2\omega+3)/2} \left[I_Q^L \right]^{1/2} \tag{26b}$$

When the limits of integration are reversed in altitude y

$$Q^L = -C_3^L \int_0^\infty e^{-(\lambda/2)y} e^{-[(2\omega+3)B/4]} e^{-\lambda y} dy \tag{27}$$

Define a laminar ballistic factor B^L as

$$B^L = \frac{(2\omega+3)}{4} B \tag{28}$$

Equation (27) can then be integrated directly to obtain

$$Q^L = \frac{C_3^L}{\lambda [B^L]^{1/2}} \gamma(1/2, B^L) \tag{29}$$

where $\gamma(1/2, B^L)$ is the incomplete gamma function.

Upon substitution for C_3^L and the definition of the incomplete gamma function, Eq. (29) may be rewritten as

$$Q^L = 0.939 \left[\frac{C_\mu \left(\frac{\gamma-1}{2\gamma R}\right) \left(\frac{\gamma+1}{\gamma-1}\right) \pi}{B^L r_B} \right]^{1/2} \left[\frac{\pi r_B^2}{\lambda \sin\theta_E} \right] \rho_o^{1/2} V_E^{(2\omega+3)/2} \left(I_Q^L \right)^{1/2} \mathrm{erf}\left(\sqrt{B^L}\right) \tag{30}$$

Finally, substituting for B^L and B from Eqs. (28) and (23a), we then have

$$Q^L = F^L \operatorname{erf}\left(\sqrt{B^L}\right) \tag{31a}$$

$$F^L = 1.866 \times 10^{-6} \left[\frac{\left(\frac{\gamma+1}{\gamma-1}\right)}{(2\omega+3)}\right]^{1/2} \left[\frac{C_\mu\left(\frac{\gamma-1}{2\gamma R}\right)^{\omega} \beta I_Q^L}{\lambda \sin\theta_E}\right]^{1/2} r_B^{3/2} V_E^{(3+2\omega)/2} \tag{31b}$$

$$\operatorname{erf}\left(\sqrt{B^L}\right) = \frac{2}{\sqrt{\pi}} \int_0^{\left(B^L\right)^{1/2}} e^{-t^2}\, dt \tag{31c}$$

E. TRAJECTORY ENVIRONMENT--TURBULENT FLOW

When we substitute for n, C_1, and C_2 in Eqs. (24) and (25)

$$\frac{dQ^T}{dy} = C_3^T e^{-(4\lambda/5)y} e^{-[(2\omega+9)B/10]e^{-\lambda y}} \tag{32a}$$

$$C_3^T = -0.0627 \left[\frac{C_\mu\left(\frac{\gamma-1}{2\gamma R}\right)^{\omega}}{r_B}\right]^{1/5} \left[\frac{\pi r_B^2 \left(\frac{\gamma+1}{\gamma-1}\right)}{\sin\theta_E}\right]^{4/5} \rho_o^{4/5} V_E^{(2\omega+9)/5} \left[I_Q^T\right]^{4/5} \tag{32b}$$

Again, if the limits of integration in altitude y are reversed

$$Q^T = -C_3^T \int_0^{\infty} e^{-(4\lambda/5)y} e^{-[(2\omega+9)B/10]e^{-\lambda y}} dy \tag{33}$$

Define a turbulent ballistic factor B^T

$$B^T = \frac{(2\omega+9)}{10} B \tag{34}$$

Integrating Eq. (33), we obtain

$$Q^T = -\frac{C_3^T}{\lambda[B^T]^{4/5}}\,\gamma(4/5, B^T) \tag{35}$$

Substituting for C_3^T, B^T and B as in the laminar case, we obtain*

$$Q^T = F^T\,\gamma(4/5,\ B^T) \tag{36a}$$

$$F^T = 4.70\times10^{-6}\left[\frac{\left(\frac{\gamma+1}{\gamma-1}\right)}{(2\omega+9)}\right]^{4/5}\left[\frac{C_\mu\left(\frac{\gamma-1}{2\gamma R}\right)^{\omega}}{\lambda\sin\theta_E}\right]^{1/5}\left(\beta I_Q^T\right)^{4/5} r_B^{9/5}\,V_E^{(9+2\omega)/5} \tag{36b}$$

where $\gamma(4/5, B^T)$ is the incomplete gamma function given by

$$\gamma(4/5, B^T) = \frac{5}{4}\int_0^{(B^T)^{4/5}} e^{-t^{5/4}}\,dt \tag{37}$$

Integrations entirely analogous to those performed on Eqs. (27) and (33), for laminar and turbulent flow, respectively, were carried out by Brunner (Refs. 2, 3). Brunner's starting point, however, was the "reference enthalpy" heat transfer expressions for laminar and turbulent flow rather than the Vaglio-Laurin expressions used herein. Also, Brunner's final results for integrated heat transfer through a trajectory were given in terms of $\mathscr{H}$, i.e., the time integrated heat transfer in Btu/ft^2 at a point on the body.

---

*Proper units for Eqs. (31a) and (36a) are discussed on page 35.

III. CALCULATED RESULTS--CONSTANT FREESTREAM ENVIRONMENT

If the freestream environment is not changing with time, then the total heat transfer rate can be expressed in terms of the freestream flowfield variables and the body geometry as given by Eqs. (10a) and (10b). These expressions are shown graphically in Fig. 1. The behavior is seen to be similar to classical Nussett number-Reynolds number behavior, with a 0.5 power Reynolds number dependence in the laminar case and a 0.2 power Reynolds number dependence in the turbulent case. Notice that the right-hand sides of Eqs. (10a) and (10b) can be interpreted as representing the fraction of the intercepted freestream total energy flux which is transferred as heat to the body.

Figure 1 is applicable for all body shapes. However, the ordinate contains the heat transfer integral I_Q, which depends upon the shape contour of the body and is given by Eq. (8).

The evaluation of I_Q reduces to evaluating the local pressure p_e at each position on the body and then integrating Eq. (8) because the normalized product $\bar{\rho}_e\bar{\mu}_e$ can be written in terms of the normalized pressure $\bar{p}_e = p_e/p_{t_2}$ as

$$\bar{\rho}_e\bar{\mu}_e = \frac{\rho_e\mu_e}{\rho_o\mu_o} = \bar{p}_e^{\,[(\gamma-1)\omega+1]/\gamma} \tag{38}$$

Also, assuming an isentropic expansion, the local velocity $\bar{u}_e$ can be written in terms of $\bar{p}_e$ as

$$\bar{u}_e = \frac{u_e}{\sqrt{2H_o}} = \sqrt{1 - \bar{p}_e^{\,(\gamma-1)/\gamma}} \tag{39}$$

Thus, I_Q is a function of the specific heat ratio γ, the temperature exponent in the viscosity law ω, and body geometry.

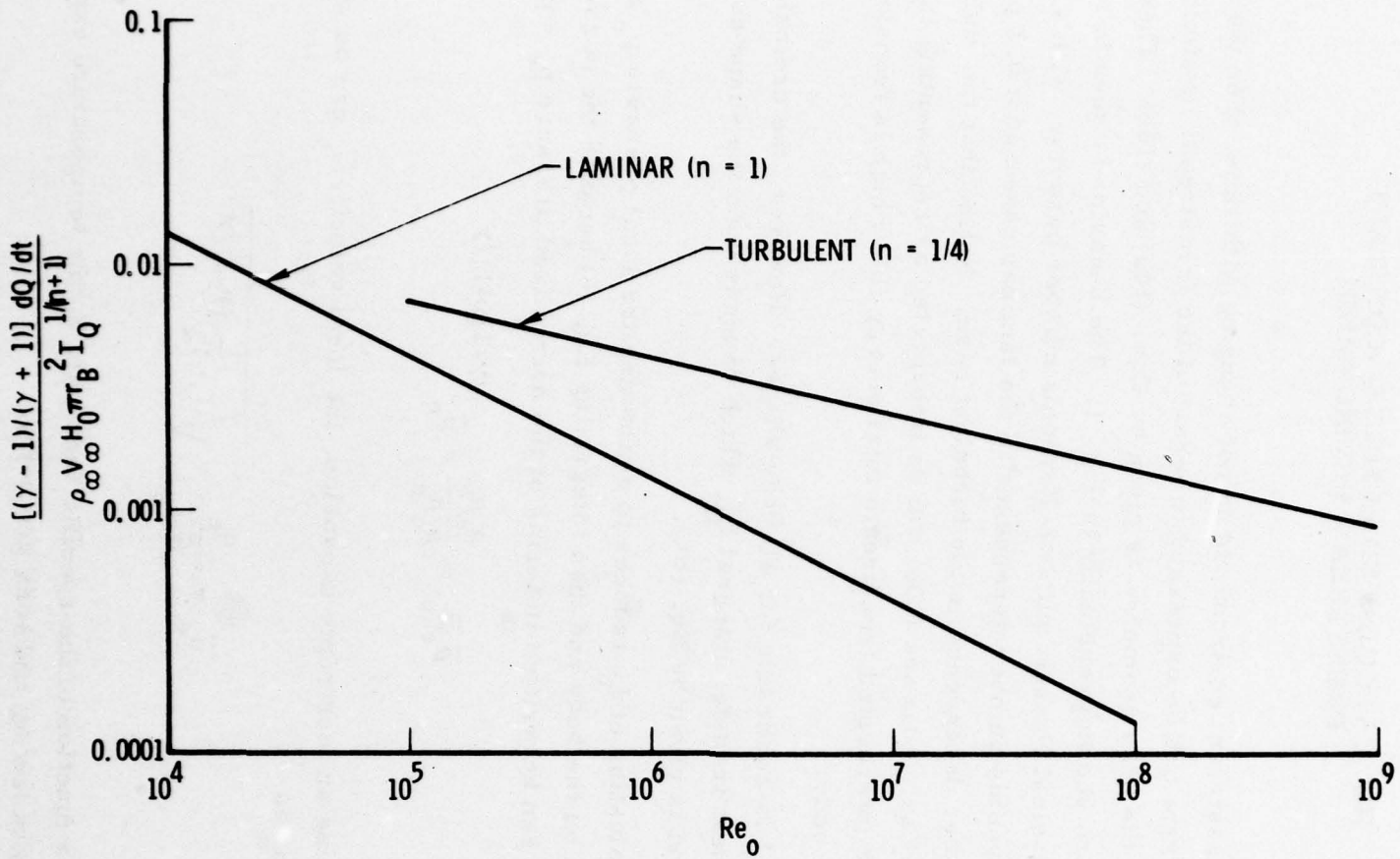

Fig. 1. Nondimensional Heat Transfer Rate as a Function of I_Q and Re_o

The inviscid flow pressure distributions needed to determine the boundary layer edge properties as given by Eqs. (38) and (39) were obtained from the best numerical inviscid flowfield calculation procedures available (Refs. 8-10). A schematic diagram of the inviscid flowfield calculation procedure for flat-face cones is shown in Fig. 2. For sphere-cones, the start line for the rotational characteristics computer program (Ref. 9) was obtained using the Ames blunt body computer program (Ref. 8).

The basic body geometry considered in this work is a cone. Calculations were carried out for cone half-angles (θ_c) of 30, 20, 10, 5 and 0 deg for both hemispherical and flat-face noses. In each instance, calculations were made by numerically integrating Eq. (8) starting at the stagnation point. Results of the numerical inviscid flowfield calculations for these geometries were used in conjunction with Eqs. (38) and (39) to evaluate the integrand along the body. In this way, I_Q^L and I_Q^T for each cone half-angle and a continuous range of thickness ratio, $\tau = 2r_B/L$, were calculated. The bluntness ratio, B.R. = r_N/r_B, and the thickness ratio are related by Eqs. (40a) and (40b). For sphere-cones

$$\text{B.R.} = \frac{\tau\cos\theta_c - 2\sin\theta_c}{\tau(1-\sin\theta_c)} \tag{40a}$$

and for flat-face cones

$$\text{B.R.} = \frac{\tau\cos\theta_c - 2\sin\theta_c}{\tau\cos\theta_c} \tag{40b}$$

---

[8] Masson, B.S., T.D. Taylor, and R.M. Foster, "Application of Godunov's Method to Blunt Body Calculations," AIAA Journal, 7(4), 1969, p. 694.

[*9] Baker, R.L., "Method of Characteristics Computer Program Including Embedded Shocks and Total Enthalpy Gradients Normal to Streamlines," Report No. ATM-71(S6816-53)-2, The Aerospace Corporation, San Bernardino, California, 3 February 1971.

[10] Inouye, M., J.V. Rakich, and H. Lomax, "A Description of Numerical Methods and Computer Programs for Two-Dimensional and Axisymmetric Supersonic Flow over Blunt-Nosed and Flared Bodies," NASA-TN-D-2970, August 1965.

[*] Aerospace internal correspondence. Not available for external distribution.

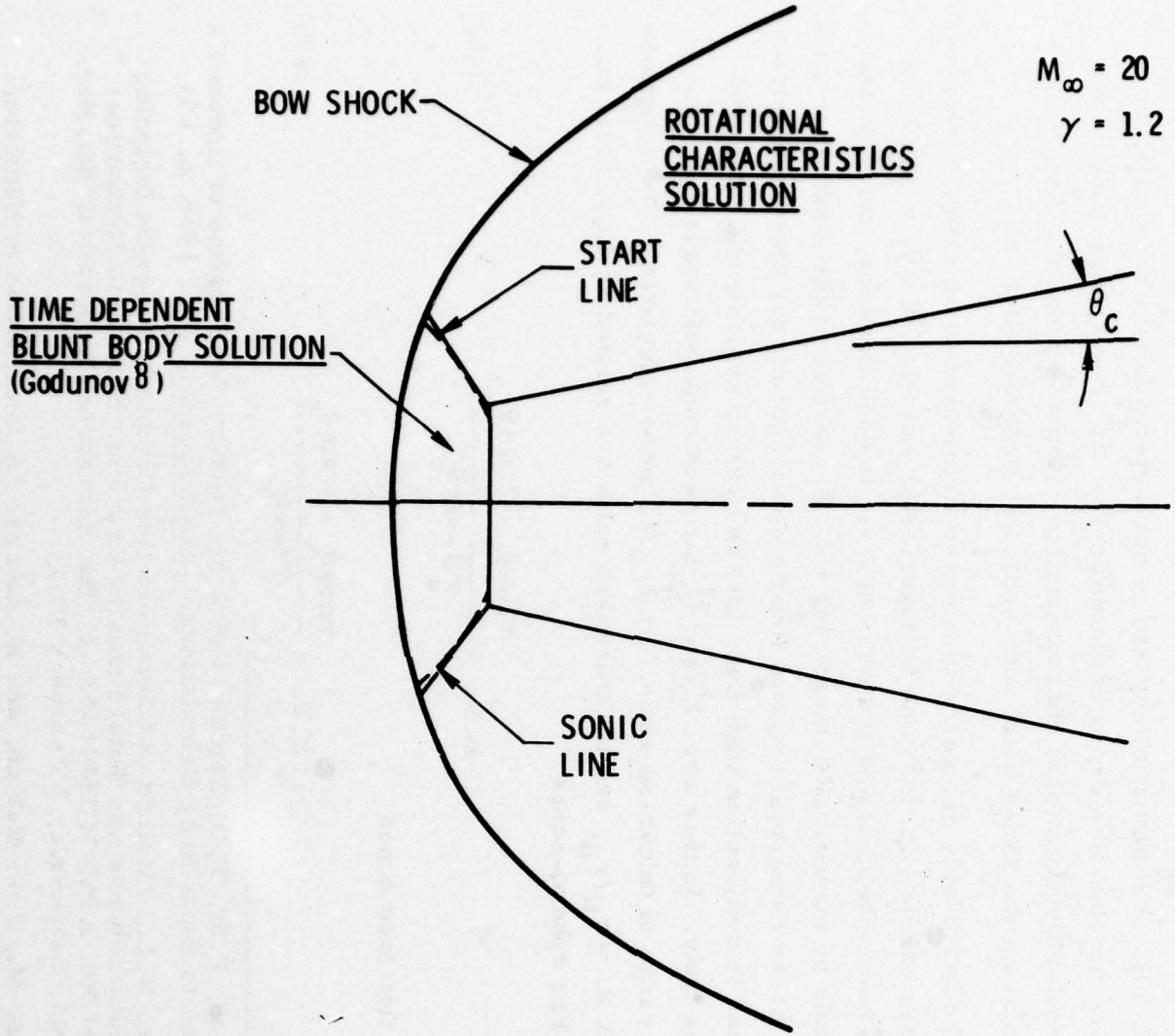

Fig. 2. Numerical Flowfield Calculation Methods

The results given in the remainder of this report are presented as a function of the thickness ratio. Through the use of Eqs. (40a) and (40b) they can easily be interpreted in terms of the bluntness ratio.

A. SPHERE-CONES

The body geometries for a family of 10-deg sphere-cones with constant base radius are shown in Fig. 3a. For $\tau \geq 2.1$, the shapes are truncated spheres and for $\tau < 2.1$ the shapes are sphere-cones with bluntness ratio decreasing as τ decreases. As the bluntness ratio B.R. approaches zero, the thickness ratio approaches the sharp cone limit

$$\tau_{\text{sharp cone}} = 2 \tan\theta_c = 0.332 \tag{41}$$

Equation (41) follows directly from Eq. (40a) for B.R. = 0.

The relationship between the integrated heat transfer rate dQ/dt, the freestream parameters ρ_∞, V_∞ and H_o, the base radius r_B, and the heat transfer integrals I_Q^L and I_Q^T is shown in Fig. 1 and is given by Eqs. (10a) and (10b). If the freestream parameters and the base radius are fixed, then the relative heat transfer rates for different bodies can be evaluated by knowing I_Q as a function of thickness ratio τ.

The I_Q^L as a function of τ for the family of 10-deg cones in Fig. 3a and all other 10-deg cones is shown in Fig. 3b. For truncated spheres, $\tau \geq 2.1$, I_Q^L is approximately constant. For sphere-cones $\tau < 2.1$, I_Q^L decreases as τ decreases due in large part to the decreasing area associated with the high heat transfer spherical cap and the fact that the inviscid flow along the cone is overexpanded. As τ continues to decrease, however, a minimum value of I_Q^L is reached. Further decrease in τ results in an increase in heat transfer because the conical region now includes flow recompression following the local overexpansion.

A sharp cone represents the smallest thickness ratio attainable for a given cone half-angle. The 10-deg sharp cone value of I_Q^L for isentropic expansion of the flow is shown by an x on Fig. 3b.

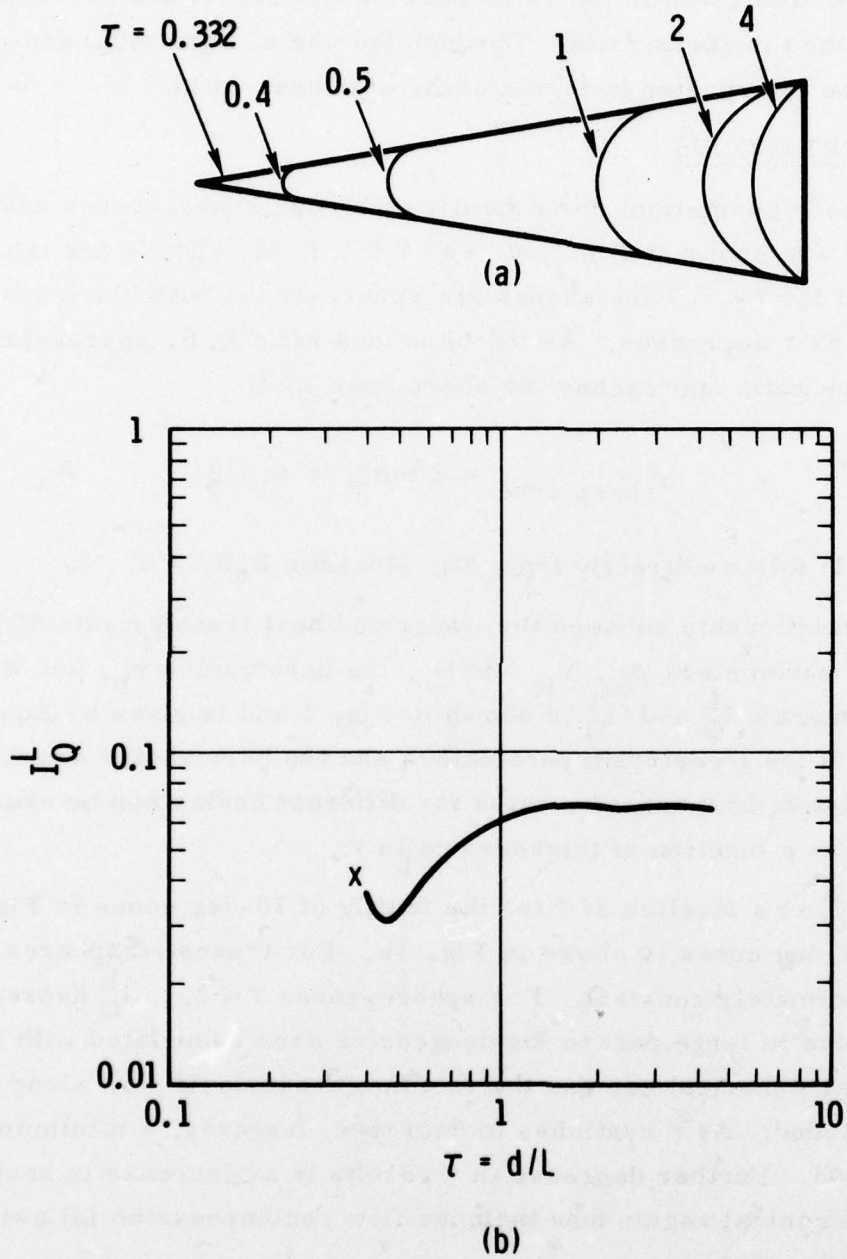

Fig. 3. Body Geometries and I_Q^L Values for 10-deg Sphere-Cones

The blunt cone calculated results are seen to be approaching the sharp cone, isentropic expansion limit as τ approaches its lower, sharp cone limit. All results presented in the remainder of this report assume isentropic expansion of the flow and are therefore applicable only when entropy swallowing effects are negligible. This is generally an excellent assumption for nosetip calculations.

Calculated values of I_Q as a function of τ for laminar and turbulent flow over sphere-cones are shown for various cone half-angles in Figs. 4a and 4b, respectively. The results are generally similar to those described in Fig. 3. For each cone half-angle greater than zero, the laminar and turbulent curves of I_Q versus τ pass through a minimum. The minimum I_Q^L or I_Q^T decreases as θ_c decreases.

To illustrate the effect of cone half-angle, bluntness ratio, and thickness ratio on the heat transfer rate, the I_Q behavior illustrated in Figs. 4a and 4b has been reproduced in Fig. 5a. The different symbols on the curves, marked by numbers, represent families of cones to be considered in the following discussion.

First consider the four • (filled circle) symbols numbered 1, 2, 3 and 4. Each point represents the minimum in the curve of I_Q^L versus τ for a particular cone half-angle. Four cones, having a constant base radius and with cone half-angles, thickness ratios and bluntness ratios corresponding to points 1 through 4, are shown in Fig. 5b. Since the base radius is constant, the intercepted freestream total energy flux is constant. However, the fraction of this flux transferred as heat to the body decreases monotonically as the cone half-angle and thickness ratio decrease, since dQ/dt is proportional to I_Q; thus

$$\frac{dQ_4}{dt} > \frac{dQ_3}{dt} > \frac{dQ_2}{dt} > \frac{dQ_1}{dt} \tag{42}$$

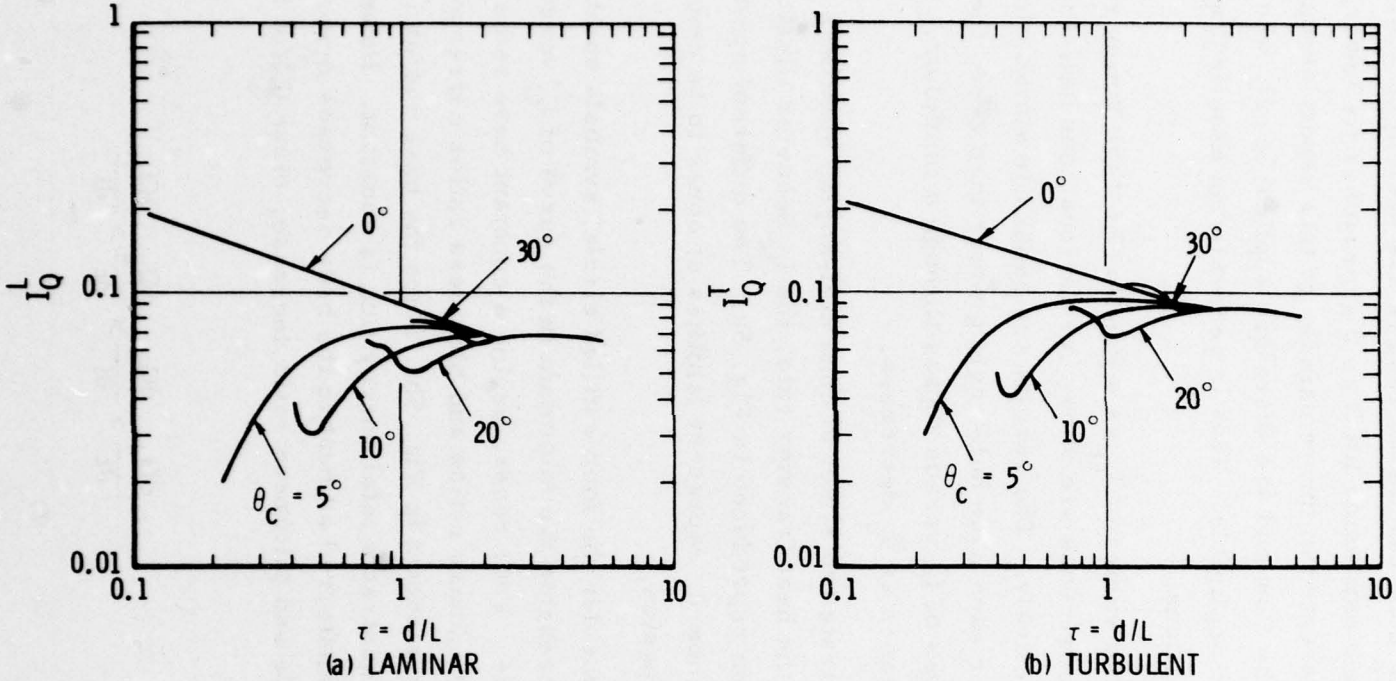

Fig. 4. I_Q as a Function of Thickness Ratio for Sphere-Cones

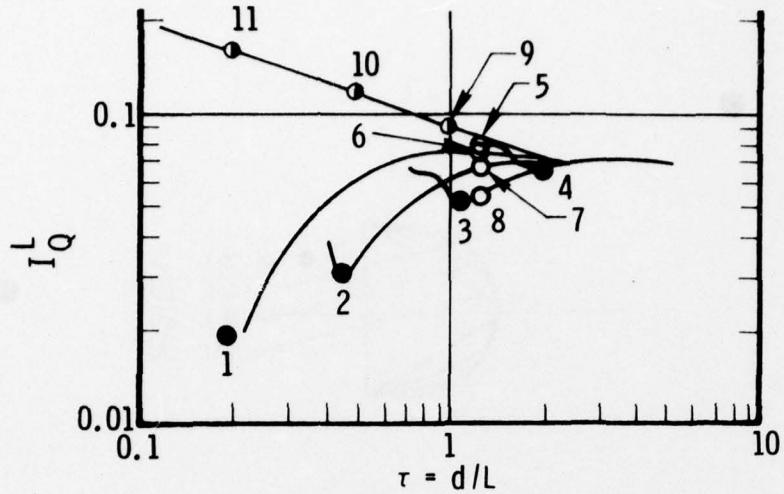

Fig. 5a. I_Q^L versus τ for Sphere-Cones

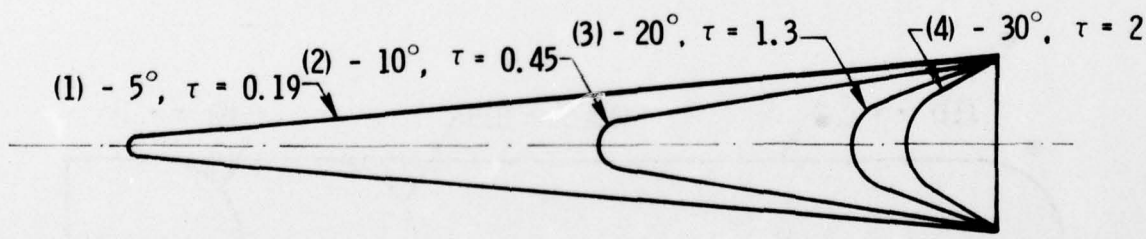

Fig. 5b. Minimum I_Q^L Cones for Various Cone Half-angles

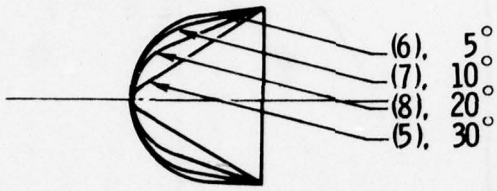

Fig. 5c. Sphere-Cones with Constant Thickness Ratio, τ = 1.3

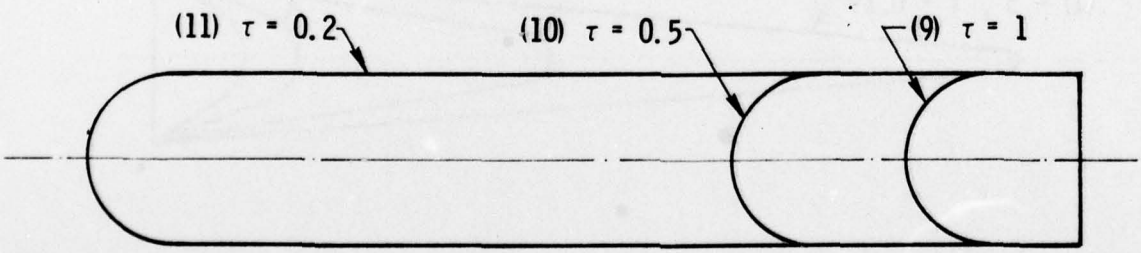

Fig. 5d. Sphere-Cylinders

The four o (open circle) symbols in Fig. 5a numbered 5, 6, 7 and 8 represent four cones having a constant thickness ratio of 1.3. These cones are illustrated in Fig. 5c. The 20-deg cone, represented by point number 8, has the lowest heat transfer rate. The 5- and 10-deg cones, points 6 and 7, have higher heat transfer rates because of larger areas associated with the high heat transfer nose cap. The 30-deg cone, point 5, also has a higher heat transfer rate because of the high conical pressure on the cone surface. Thus, for these cones

$$\frac{dQ_5}{dt} > \frac{dQ_6}{dt} > \frac{dQ_7}{dt} > \frac{dQ_8}{dt} \tag{43}$$

The behavior of I_Q versus τ for a sphere-cylinder can now be understood by considering Fig. 5d and the ⊖ (half-filled circle) symbols in Fig. 5a, points 9, 10 and 11. We see in Fig. 5d that body 9 may be considered a part of body 10. Likewise, bodies 9 and 10 may be considered parts of body 11. Therefore, going from body 9 to body 10 and then to body 11, the total heat transfer must increase or

$$\frac{dQ_{11}}{dt} > \frac{dQ_{10}}{dt} > \frac{dQ_9}{dt} \tag{44}$$

B. FLAT-FACE CONES--COMPARISON WITH SPHERE-CONES

Calculated values of I_Q for laminar and turbulent flow over flat-face cones are shown for various cone half-angles in Figs. 6a and 6b, respectively. The behavior is comparable to that for sphere-cones as shown in Figs. 4a and 4b with some notable differences. The surface pressure distributions for a 10-deg sphere-cone and a 10-deg flat-face cone are compared in Fig. 7. Since I_Q depends upon the pressure distribution through Eqs. (38) and (39), differences in the pressure distributions will be reflected in the I_Q versus τ behavior. The major difference between the sphere-cone and the flat-face cone pressure distributions is in the region of $x/r_n < 1.0$. The rapid

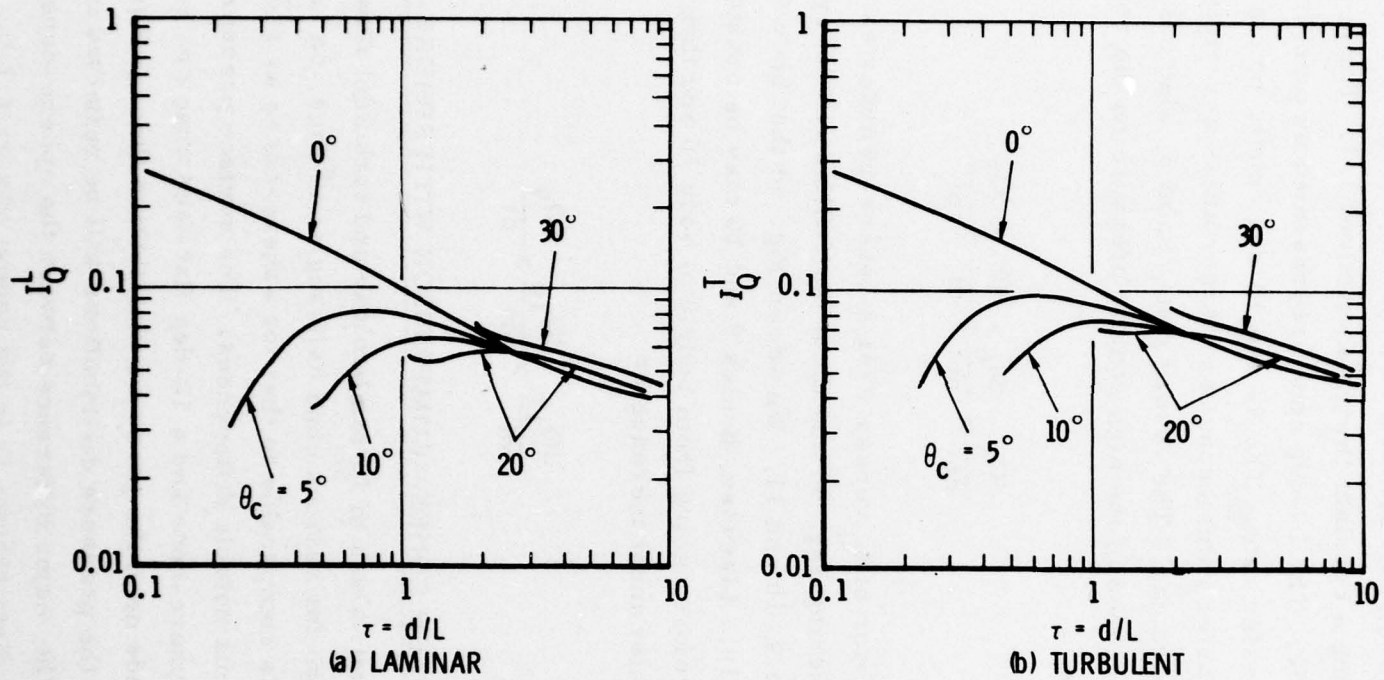

Fig. 6. I_Q as a Function of Thickness Ratio for Flat-face Cones

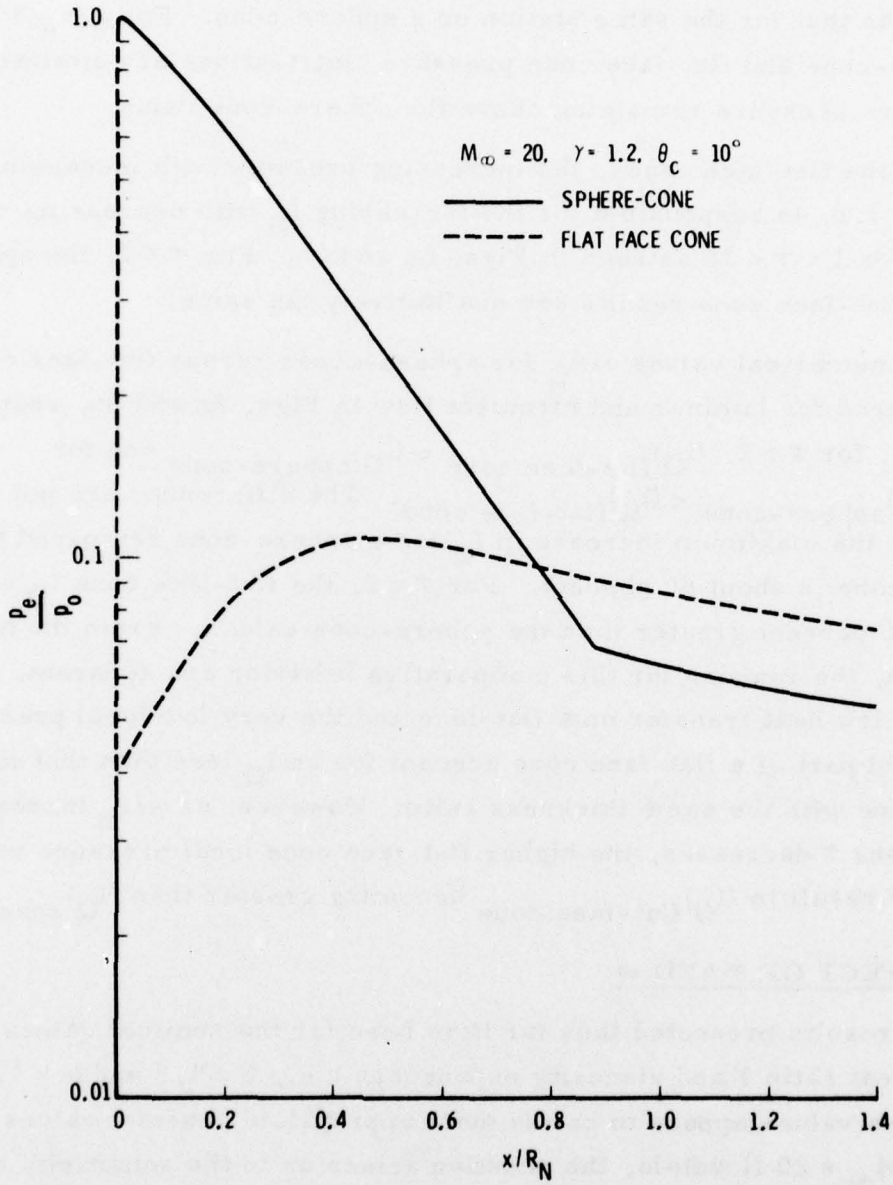

Fig. 7. Surface Pressure Distributions

expansion of the flow at the corner of the flat-face cone results in a severe local overexpansion with immediate recompression to a pressure level greater than that for the same station on a sphere-cone. For $x/r_n > 1$, the sphere-cone and flat-face cone pressure distributions are similar, with the flat-face pressure remaining above the sphere-cone value.

For the flat-face cones, the increasing pressure with increasing x/r_n for $x/r_n < 1.0$, is responsible for the increasing I_Q with decreasing τ behavior for $1 < \tau < 10$ as seen in Figs. 6a and 6b. For $\tau < 1$, the sphere-cone and flat-face cone results are qualitatively the same.

The numerical values of I_Q for sphere-cones versus flat-face cones are compared for laminar and turbulent flow in Figs. 8a and 8b, respectively. In general, for $\tau > 2$, $(I_Q)_{\text{flat-face cone}} < (I_Q)_{\text{sphere-cone}}$ and for $\tau < 2$, $(I_Q)_{\text{sphere-cone}} < (I_Q)_{\text{flat-face cone}}$. The differences are not large. For $\tau > 2$, the maximum increase in I_Q for a sphere-cone compared to a flat-face cone is about 50 percent. For $\tau < 2$, the flat-face cone I_Q values are 5 to 30 percent greater than the sphere-cone values. From the above discussion, the reasons for this comparative behavior are apparent. The relatively low heat transfer on a flat-face and the very low local pressures on the forward part of a flat-face cone account for an I_Q less than that for a sphere-cone with the same thickness ratio. However, as x/r_n increases, which means τ decreases, the higher flat-face cone local pressure values eventually result in $(I_Q)_{\text{flat-face cone}}$ becoming greater than $(I_Q)_{\text{sphere-cone}}$.

C. EFFECT OF γ AND ω

All results presented thus far have been for the nominal values of specific heat ratio γ and viscosity exponent ω; i.e., $\gamma = 1.2$ and $\omega = 1.0$. While these values appear to be the most appropriate constant values for the selected $M_\infty = 20$ flowfield, the question arises as to the sensitivity of the results to changes in these nominal values. To illustrate the sensitivity, calculated results are presented in Fig. 9 showing I_Q^L for 10-deg sphere-cones,

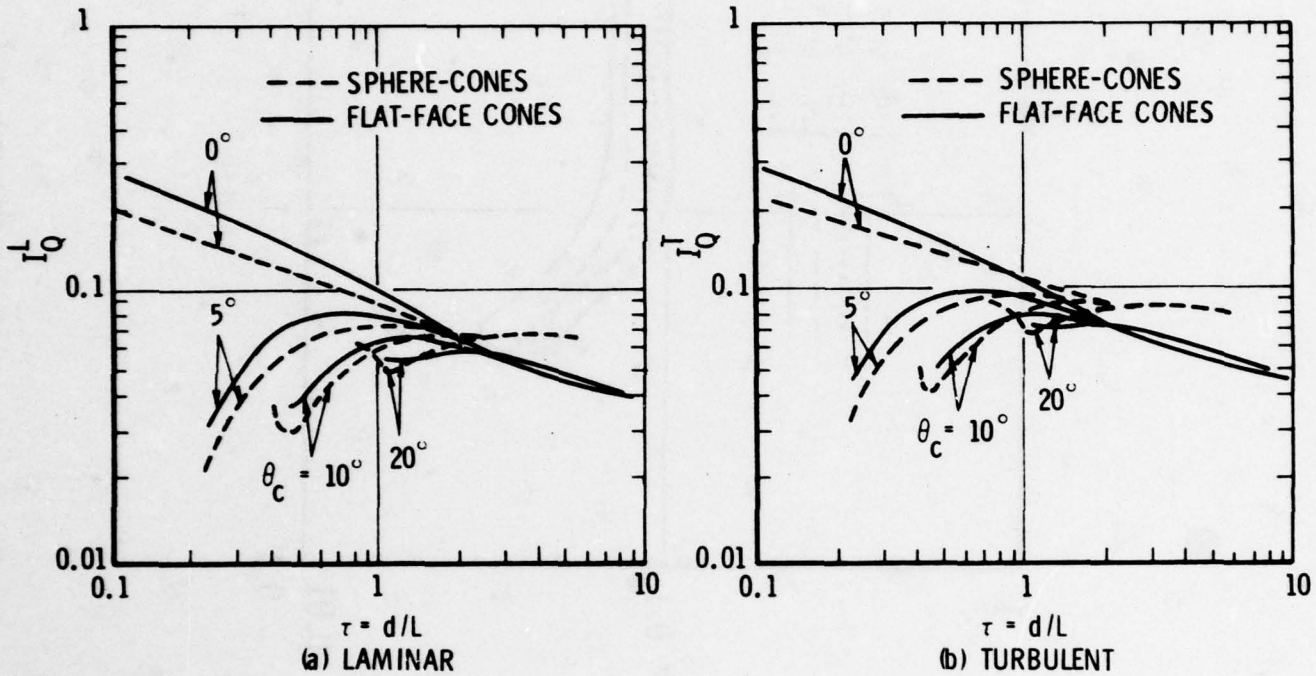

Fig. 8. I_Q versus τ for Sphere-Cones and Flat-face Cones

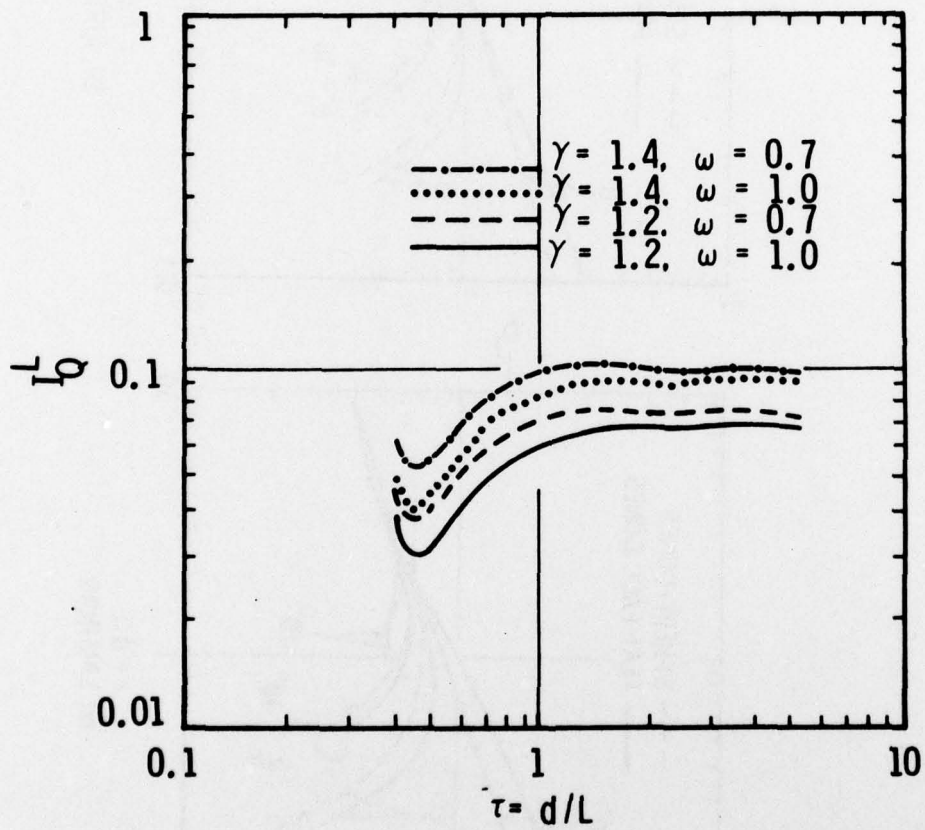

Fig. 9. Sensitivity of L_Q^L to γ and ω, 10-deg Sphere-Cone

for all combinations of $\gamma = 1.2$ or 1.4 and $\omega = 1.0$ or 0.7. Both increasing γ from its nominal value and decreasing ω from its nominal value result in an increase in I_Q^L. The highest I_Q^L value for given τ occurs for $\gamma = 1.4$ and $\omega = 0.7$.

The heat transfer rate dQ^L/dt is proportional to $\left[I_Q^L / Re_o\right]^{1/2}$ as given by Eqs. (10a). The Re_o is given as a function of γ and ω by Eq. (20a). Combining Eqs. (10a), (20a) and the results of Fig. 9, we conclude that

$$\left[\frac{\left(dQ^L/dt\right)_{\gamma=1.4,\omega=0.7}}{\left(dQ^L/dt\right)_{\gamma=1.2,\omega=1.0}}\right]_{max} = 1.576 \tag{45a}$$

Similarly

$$\left[\frac{\left(dQ^T/dt\right)_{\gamma=1.4,\omega=0.7}}{\left(dQ^T/dt\right)_{\gamma=1.2,\omega=1}}\right]_{max} = 1.161 \tag{45b}$$

IV. CALCULATED RESULTS--TRAJECTORY ENVIRONMENT

A. LAMINAR OR TURBULENT FLOWS

In this case, the total heat transfer is given by Eqs. (31a) and (36a) for laminar and turbulent flow, respectively. From these equations, we see that for specified reentry conditions and vehicle ballistic coefficient the total heat transfer Q depends on the body shape and the body scale through the parameters I_Q and r_B, respectively. Since the I_Q's in Eqs. (31a) and (36a) are the same as those in Eqs. (10a) and (10b), results discussed above in conjunction with Figures 3 through 9 are also directly applicable to the present case. Thus, Figs. 4 and 6 supply the values of I_Q^L and I_Q^T to be used in Eqs. (31a) and (36a) to evaluate Q^L and Q^T for sphere-cones and flat-face cones, respectively. Also needed are the values of the functions containing the ballistic parameters B^L and B^T, i.e., $\mathrm{erf}\sqrt{B^L}$ and $\gamma(4/5, B^T)$. These functions are shown in Fig. 10.

If the calculated results given in Figs. 4, 6, and 10 are used in combination with Eqs. (31a) and (36a), the total heat Q[Btu] transferred to a nose tip or a reentry vehicle for a complete reentry trajectory can be easily calculated. The appropriate units for the parameters in Eqs. (31a) and (36a) are $C_\mu[0.979 \times 10^{-8}\ (\mathrm{lb_m/ft\text{-}sec\text{-}^oR})]$, $\beta\,[\mathrm{lb_m/ft^2}]$, $\lambda\,[\mathrm{ft^{-1}}]$, $r_B[\mathrm{ft}]$, $V_E[\mathrm{ft/sec}]$.

If the nose tip heat transfer is desired, then the r_B used in these equations should be the "base" radius of the nose tip, and the thickness ratio τ used to evaluate I_Q from the figures should be that for the nose tip. Likewise, for evaluating the total heat transferred to the entire reentry vehicle, the r_B and τ should correspond to the entire vehicle values of these parameters.

Caution must be applied in using the results calculated in the preceding manner if the bluntness ratio B.R. = r_N/r_B of the nose tip or vehicle is less than 0.1, since entropy swallowing effects are then likely to be important.

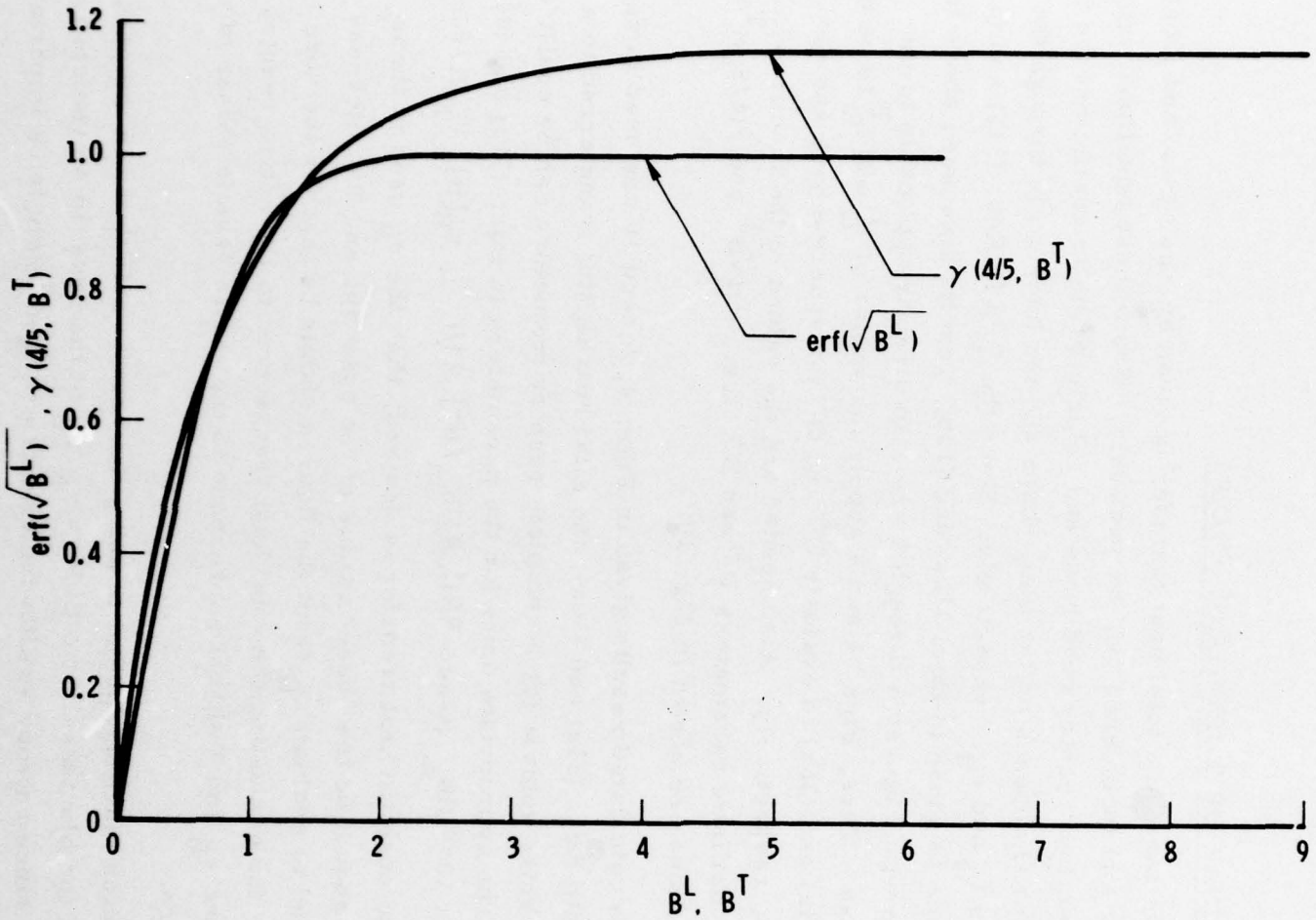

Fig. 10. Laminar and Turbulent Heat Transfer Functions

B. LAMINAR-TURBULENT FLOW

The above procedures allow the calculation of the total heat transfer Q only for those cases in which the flow in the boundary layer is all-laminar or all-turbulent for the entire trajectory. If, when boundary layer transition occurs, it is assumed that the flow changes instantaneously from laminar to turbulent over the whole nose tip or vehicle, then the total laminar-turbulent heat transfer Q^{LT} can be evaluated.

For the laminar-turbulent case with boundary layer transition occurring at altitude h we have

$$Q^{LT} = \int_{\infty}^{h} \frac{dQ^L}{dy}\, dy + \int_{h}^{0} \frac{dQ^T}{dy}\, dy \tag{46}$$

The details of performing these integrations are given in Appendix A. The final result is

$$Q^{LT} = F^L \operatorname{erf} \sqrt{B_p^L} + F^T \left\{ \gamma\left(4/5, B^T\right) - \gamma\left(4/5, B_p^T\right) \right\} \tag{47}$$

where F^L and F^T are defined by Eqs. (31b) and (36b), respectively, and the partial trajectory ballistic factors B_p^L and B_p^T are given by

$$B_p^L = B^L e^{-\lambda h} \tag{48a}$$

$$B_p^T = B^T e^{-\lambda h} \tag{48b}$$

Thus, Q^{LT} is evaluated in the same manner as Q^L and Q^T except multiple use of Fig. 10 is required to give the three components. From either Q^L, Q^T, or Q^{LT}, the total mass of an ablating material lost during a reentry trajectory is given by

$$M = \frac{Q}{Q^*}$$

where Q^* is the cold wall effective heat of ablation.

C. EVALUATING LOCAL HEAT LOADS

In many instances, it is desirable to know the total local heat load at a particular body station in comparison to the total body heat load. The total local heat load $\mathscr{H}$ is related to the total body heat load Q by

$$\mathscr{H} = \frac{1}{2\pi r} \frac{dQ}{ds} \tag{49}$$

Expressions for dQ/ds may easily be obtained from Eqs. (31a) and (36a) for laminar and turbulent flow, respectively. In these equations, I_Q^L and I_Q^T are the only variables which are a function of s. Performing the indicated differentiation and substituting into Eq. (49), we obtain for laminar flow

$$\mathscr{H}^L = 1.443 \times 10^{-7} \left[\frac{\left(\frac{\gamma+1}{\gamma-1}\right)}{(2\omega+3)}\right]^{1/2} \left\{\frac{C_\mu \left(\frac{\gamma-1}{2\pi R}\right)^\omega \beta}{\lambda \sin\theta_E r}\right\}^{1/2} V_E^{(3+2\omega)/2} q^L \operatorname{erf}\left(\sqrt{B^L}\right) \tag{50a}$$

and for turbulent flow

$$\mathscr{H}^T = 1.691 \times 10^{-7} \left[\frac{\left(\frac{\gamma+1}{\gamma-1}\right)}{(2\omega+9)}\right]^{4/5} \left\{\frac{\left[C_\mu \left(\frac{\gamma-1}{2\pi R}\right)^\omega\right]^{1/5} \beta^{4/5}}{\left[\lambda \sin\theta_E r\right]^{1/5}}\right\} V_E^{(9+2\omega)/5} q^T \gamma(4/5, B^T) \tag{50b}$$

The nondimensional heat transfer parameters q^L and q^T are given by

$$q^L = \frac{\bar{\rho}_e \bar{u}_e \bar{\mu}_e \bar{r}}{\left(I_Q^L\right)^{1/2}} \tag{51a}$$

$$q^T = \frac{\bar{\rho}_e \bar{u}_e \bar{\mu}_e \bar{r}^{1/4}}{\left[I_Q^T\right]^{1/5}} \tag{51b}$$

Comparing Eqs. (51a) and (51b) with Eqs. (1a) and (1b), we see that q^L and q^T are simply nondimensional representations of the original Vaglio-Laurin laminar and turbulent heat flux expressions.

In Eqs. (50a) and (50b), q^L and q^T have been normalized in such a way that q^L is unity at an axisymmetric stagnation point and q^T is unity at the maximum turbulent heating point on a sphere. The parameters q^L and q^T have been calculated and are shown in Figs. 11 and 12 for sphere-cones and flat-face cones, respectively. Notice that the reference length in Eqs. (51a) and (51b) is the nose radius or flat-face step height, designated r_N.

We are now in a position in which it is possible to easily compare the present results with those of Brunner. Recall that Brunner's starting point was the flat-plate-reference-enthalpy heat transfer expressions, whereas the present starting point has been the Vaglio-Laurin equations. The detailed algebraic manipulations for this comparison are given in Appendix B. The laminar total local heat transfer $\mathscr{H}^L$ given by Eq. (50a) is for an axisymmetric stagnation point 11.1 percent lower than that calculated from Brunner's expression. The turbulent total local heat transfer $\mathscr{H}^T$, given by Eq. (50b) for the maximum turbulent heating point on a sphere, is 14.9 percent higher than that calculated from Brunner's equation.

For an ablating material, the total recession depth d at a given nose tip or body location can be calculated from

$$d = \frac{\mathscr{H}}{\rho_b Q^*} \tag{52}$$

where ρ_b is the bulk density of the ablating material and Q^* is the cold wall effective heat of ablation. If Figs. 11 and 12 are used, the d for any location on the families of sphere-cones and flat-faced cones considered in this work can be easily calculated.

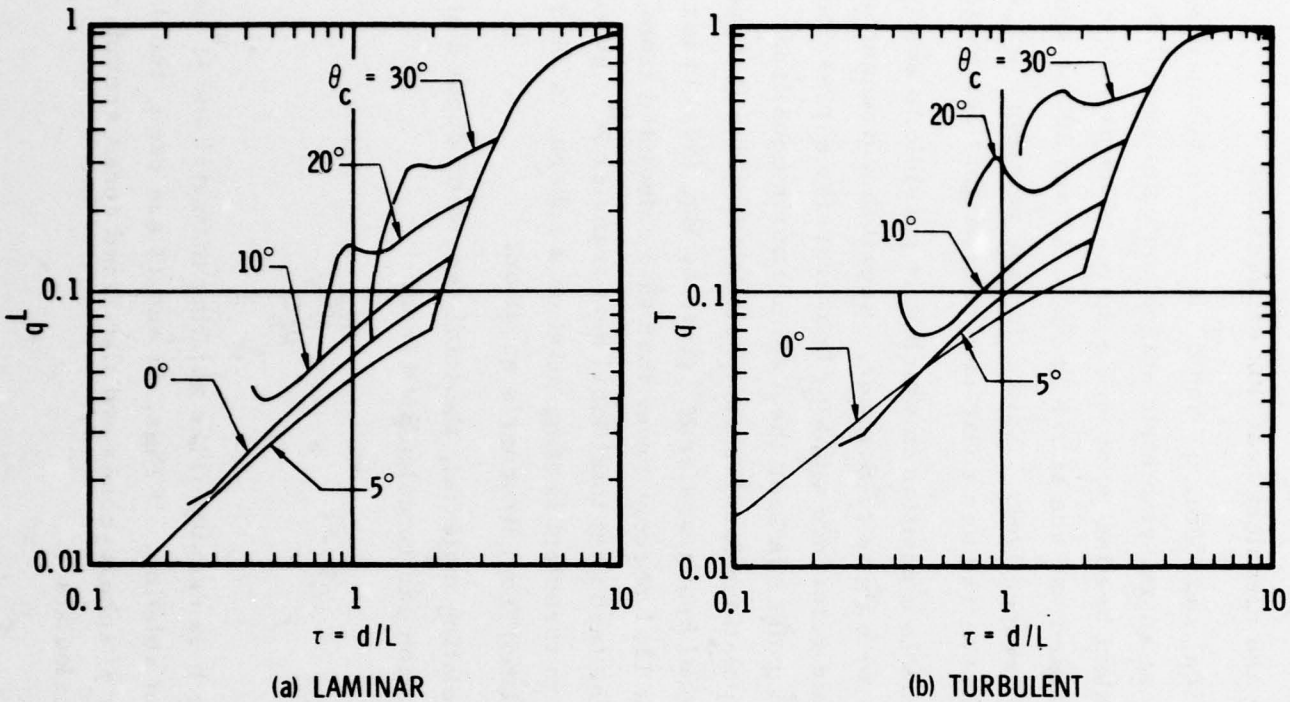

Fig. 11. Local Heat Transfer Functions, Sphere-Cones

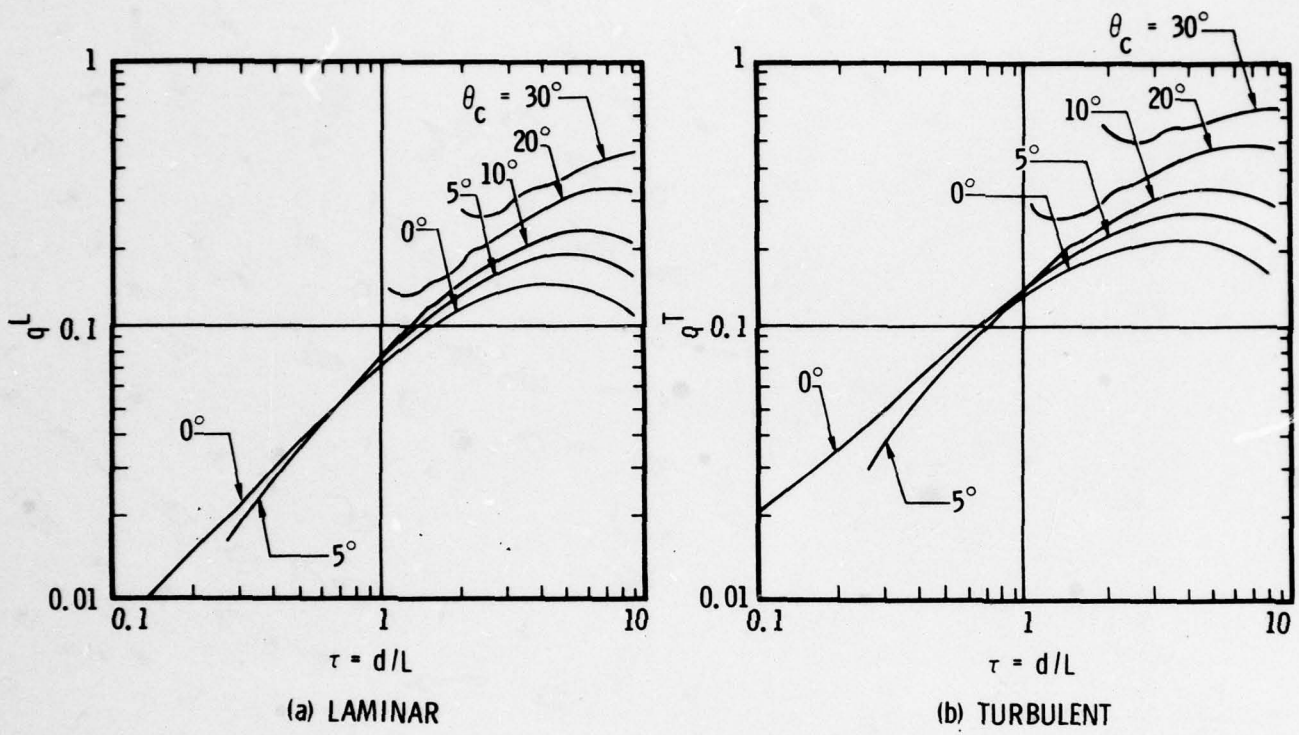

Fig. 12. Local Heat Transfer Function, Flat-face Cones

V. SUMMARY

Beginning with the hypersonic convective heat transfer expressions for laminar and turbulent flow given by Vaglio-Laurin, equations for the total heat transfer to a body in a hypersonic flow environment have been derived. When these equations are used together with the graphical results presented, total heat transfer to selected body geometries can be calculated directly. Both the case of a constant, ground test type environment and a realistic reentry vehicle trajectory environment have been considered.

The total heat transfer is given as a function of freestream or reentry parameters, body scale and heat transfer integrals which are functions of the body geometry. The best available inviscid flow field calculation methods for surface pressure distributions were used to calculate the laminar and turbulent heat transfer integrals I_Q^L and I_Q^T for 0-, 5-, 10-, 20-, and 30-deg sphere-cones and flat-face cones. These results are presented graphically as a function of the fineness ratio, i.e., the diameter to length ratio. From these figures, the variation of total heat transfer with nose bluntness ratio, fineness ratio, and cone half-angle has been examined.

For the trajectory environment, in addition to total laminar or turbulent heat transfer prediction methods, a method for evaluating the total heat transfer for laminar flow to boundary layer transition altitude and all turbulent flow to impact is also given. When the total heat load to the body or nose tip is known, the heat shield weight or transpiration nose tip coolant requirements can be directly calculated.

Finally, graphical results giving the distribution functions for local laminar and turbulent heat transfer over the sphere-cone and flat-face cone geometries considered in this work are given. These results allow the total local heat load at selected axial stations, and therefore the local depth of heat shield ablation, to be calculated.

APPENDIX A

DERIVATION OF Q^{LT} RELATIONSHIP

For a laminar-turbulent trajectory case, Q^{LT} is evaluated by performing the integrations indicated by Eq. (46). The integrand dQ^L/dy is given by Eq. (26a) and dQ^T/dy is given by Eq. (32a). These integrands have already been integrated between the limits of zero and infinity with the final results given by Eqs. (31a) and (36a). We now consider the partial integrations.

First, for the laminar portion of the trajectory

$$Q_p^L = \int_{\infty}^{h} C_3^L e^{-\lambda y/2} e^{-B^L e^{-\lambda y}} dy \tag{A-1}$$

When the substitution $t = \sqrt{B^L} e^{-\lambda y/2}$ is made, Eq. (A-1) may be rewritten as

$$Q_p^L = \frac{-C_3^L \sqrt{\pi}}{[B^L]^{1/2}\lambda} \left[\frac{2}{\sqrt{\pi}} \int_0^{\sqrt{B^L} e^{-(\lambda h)/2}} e^{-t^2} dt \right] \tag{A-2}$$

Equation (A-2) is the same form as Eq. (31c) except that the upper limit of integration is different. Thus, we define B_p^L by

$$B_p^L = B^L e^{-\lambda h} \tag{A-3}$$

The integral in Eq. (A-2) is thus represented by the error function of argument $\sqrt{B_p^L}$ and the first term in Eq. (47) is obtained after appropriate substitutions.

For the turbulent portion of the trajectory

$$Q_p^T = \int_h^0 C_3^T e^{-(4\lambda/5)y} e^{-B^T e^{-\lambda y}} dy \tag{A-4}$$

When the substitution $t = [B^T]^{4/5} e^{-4\lambda y/5}$ is made, Eq. (A-4) becomes

$$Q_p^T = \frac{-5C_3^T}{4\lambda[B^T]^{4/5}} \int_{[B^T]^{4/5} e^{-(4\lambda/5)h}}^{[B^T]^{4/5}} e^{-t^{5/4}} dt \tag{A-5a}$$

or

$$Q_p^T = \frac{-5C_3^T}{4\lambda[B^T]^{4/5}} \left\{ \int_0^{[B^T]^{4/5}} e^{-t^{5/4}} dt - \int_0^{[B^T]^{4/5} e^{-(4\lambda/5)h}} e^{-t^{5/4}} dt \right\} \tag{A-5b}$$

The first term of Eq. (A-5b) is the same as Eq. (37). The second term differs only in the upper limit of integration. Thus, we define B_p^T by

$$B_p^T = B^T e^{-\lambda h} \tag{A-6}$$

Then with the definition

$$\gamma\left(4/5, X\right) = \frac{5}{4} \int_0^{[X]^{4/5}} e^{-t^{5/4}} dt \tag{A-7}$$

the last two terms in Eq. (47) follow directly from Eq. (A-5b) after appropriate substitution.

APPENDIX B

COMPARISON WITH BRUNNER'S WORK

The major thrust of the present work has been to obtain Eqs. (31a) and (36a), which give the total heat transfer values Q^L and Q^T. These equations were obtained by performing successive body surface and time (altitude) integrations of the appropriate local heat transfer rate and altitude-dependent expressions for heat transfer. Brunner's work involved only the time (altitude) integrations of the local heat transfer rate to obtain $\mathscr{H}$, the total trajectory integrated heat transfer at a point on the body.

As indicated by Eq. (49), $\mathscr{H}$ and Q are related by

$$\mathscr{H} = \frac{dQ/ds}{2\pi r} \tag{B-1}$$

Since the starting point of the present work is the Vaglio-Laurin convective heat transfer relationships, and Brunner's starting point was the flat-plate reference enthalpy heat transfer expressions, it is of interest to compare the values of $\mathscr{H}$ obtained from the two methods.

For convenience, we define the following:

$\mathscr{H}_1$ - $\mathscr{H}$ evaluated using Brunner's equations

$\mathscr{H}_2$ - $\mathscr{H}$ evaluated using the present equations

The $\mathscr{H}_2^L$ and $\mathscr{H}_2^T$ are given by Eqs. (50a) and (50b), respectively. If the present notation is used, Brunner's expressions are given by

$$\mathscr{H}_1^L = 4.155 \times 10^{-10} \left\{ \frac{\pi\beta}{1.1\lambda \sin\theta_E r_N} \right\}^{1/2} V_E^{2.2} \operatorname{erf}(\sqrt{1.1B}) \tag{B-2a}$$

$$\mathscr{H}_1^T = 2.392 \times 10^{-10} \left\{ \frac{\beta^{4/5}}{\left[\lambda \sin\theta_E r_N\right]^{1/5}} \right\} V_E^{2.48} \gamma(4/5, 1.24B) \tag{B-2b}$$

A direct numerical comparison of the two methods is now possible. Equations (B-2a) and (B-2b) are for an axisymmetric stagnation point and the maximum turbulent heating point on a sphere, respectively. Thus, we set q^L and q^T in Eqs. (50a) and (50b) to unity. Note also that the exponents on β, λ, $\sin\theta_E$ and r_N are the same in Eqs. (B-2a) and (50a) for laminar flow and in Eqs. (B-2b) and (50b) for turbulent flow. Forming the ratio $\mathscr{H}_2/\mathscr{H}_1$ and substituting from these equations, we obtain for a laminar stagnation point on a sphere

$$\frac{\mathscr{H}_2^L}{\mathscr{H}_1^L} = \frac{1.61}{1.811} = 0.889 \qquad \text{(B-3a)}$$

and for the turbulent maximum heating point on a sphere

$$\frac{\mathscr{H}_2^T}{\mathscr{H}_1^T} = \frac{12.75}{11.1} = 1.149 \qquad \text{(B-3b)}$$

For these numerical evaluations, the following input quantities were assumed:

$$\begin{aligned} \gamma &= 1.2 \\ \omega &= 1.0 \\ V_E &= 20{,}000 \text{ ft/sec} \\ B &= 1.0 \\ C_\mu &= 0.979 \times 10^{-8} \frac{\text{lb}_m}{\text{ft-sec-}^\circ\text{R}} \end{aligned} \qquad \text{(B-4)}$$